Long distance chemical gradient induced by surface nanocrystallization

Qingqing Sun [a,b], Rong Xu [c], Qingyou Han [a,*], Kejie Zhao [c], Ian McAdams [a], Wilson Xu [a]

[a] School of Engineering Technology, Purdue University, West Lafayette, IN 47907, USA
[b] School of Chemistry and Chemical Engineering, Central South University, Changsha, Hunan 410012, China
[c] School of Mechanical Engineering, Purdue University, West Lafayette, IN 47907, USA

A B S T R A C T

Natural structures are wonderful examples of what can be done with a fairly limited selection of resources. Natural structures have this feature due to their complex architecture, gradient chemical compositions and microstructure. Inspired by nature, many attempts have been made to manufacture man-made materials with similar gradients (e.g. surface nanocrystallization by severe surface plastic deformation (S^2PD)). Gradient microstructure of alloys manufactured by the S^2PD techniques has been very well studied. However, the distribution of chemical compositions within the alloy after the S^2PD treatment has rarely been explored. The current work found that by using S^2PD combined with one-year long natural aging treatments, the microstructure and chemical composition of the Al-Zn-Mg-Cu alloy (7034 Al alloy) exhibited a new gradient distribution measured from the treated surface to the pristine interior. Zn (Cu) content on the surface layer increased from 10.2 (1.3) to 57.7 (5.9) wt.%, along with an Mg surface layer depletion after treatments. The thickness of the observed chemical gradient layer was surprisingly as thick as 45 μm. Also observed were the similar phenomena in other alloys after the same treatments. The findings provide potential improvements in bioinspired materials manufacturing, rare resource saving and surface functionalization.

© 2018 Elsevier Ltd. All rights reserved.

1. Introduction

The art of metal design relies heavily on alloying. By adding other elements into a metal, desired properties and performances can be achieved. For instance, ultrahigh strength aluminum alloys used for aircrafts are hardened by nano-sized precipitates containing magnesium, copper and zinc. By alloying tungsten with nickel-molybdenum-chromium, a superalloy has been designed with excellent corrosion resistance in a wide range of severe environments. However, in many cases, alloying with elements is impractically expensive. One of the strategies to meet the increasing burden of rare resources is by learning lessons from nature [1,2]. The main concept is that resource utilization can be efficiently accomplished through the use of gradient materials. The appendages of the mantis shrimp is an excellent example of biological material being utilized with a mixture of chemical and microstructural gradients [1,3,4]. Within the shrimp's appendage, a primary chemical gradient exists between the impact and periodic regions of the appendage with the former markedly abundant in calcium and phosphorous yet deficient in carbon and magnesium.

The thickness of chemical gradient is approximately 50–100 μm. The crystallinity also increases along the same direction, yet the crystallite size decreases simultaneously. The final result of the combination of these multiple gradients is a remarkably resilient and damage tolerant weapon that can be used repeatedly for high impact hunting. Chemical gradient is also found in other biosystems, such as spider fangs [5] (~50 μm in thickness), the jaws of bloodworm *Glycera dibranchiate* [6] (~25 μm in thickness), the adhesive tarsal setae of ladybird beetle *Coccinella septempunctat* [7] (~50 μm in thickness).

Unlike biological materials, structures/compositions/textures of metallic structural materials like deformed steel sheets are usually the same for surface layer and interior part. However, inspired by nature's example, attempts such as high-temperature impregnation [8], ion beam doping [9], nitriding [10] and additive manufacturing [11] have been used to synthesize materials with gradient composition/microstructure/function over the past two decades [1,2,12]. S^2PD technologies have been utilized to generate nanocrystalline microstructures on the surface layer of many alloys with bulk coarsened grains [10,13–21]. The grain size gradient ranged from nanoscale on the surface to a microscale interior which provides materials with a combination of higher strength and adequate ductility [14]. Cracks can be arrested and fatigue resistance significantly improved due to grain refinement

* Corresponding author.
  E-mail address: hanq@purdue.edu (Q. Han).

and the induced compressive residual stress in peened specimens [15]. In addition to the previously mentioned advantages, surface nanocrystallization can specially facilitate additional surface treatments. For example, the treatment can increase the nitriding rate or decrease nitriding temperature significantly. The phenomenon is due to the fact that the resulting high density grain boundaries and/or dislocations act as "short circuit" paths for diffusion [10]. As proposed by Lu et al. [22], this defect-engineering strategy makes high-performance metals less relying on alloying. However, compared with the literature found on biological materials usually combining gradients of composition and microstructure together, the distribution of chemical compositions within the alloy after the S²PD treatment has rarely been explored [10,13–21].

The current work exhibits a gradient composition distribution in an alloy that is a result of a surface nanocrystallization followed by an ageing treatment. The chemical composition distributions were compared within the Al-Zn-Mg-Cu (7034 Al alloy) alloys before and after treatment with ultrasonic shot peening (USSP). The details of materials preparation and USSP treatment can be seen in the Experimental section. After USSP and one year of natural ageing treatments, Zn (Cu) content on surface layer increased from 10.2 (1.3) to 57.7 (5.9) wt.%; On the contrary, Mg was depleted on the surface layer after the treatments. The thickness of the layer with the gradient composition reached up to 45 μm, which is comparable to that of biological materials [1,3–6]. The current work reports, for the first time to our knowledge, the coexistence of a gradient distribution of chemical compositions and microstructures in a relatively long distance (∼45 μm) within alloys treated by S²PD. The authors believe that this study is a timely contribution to understanding of the physiochemical behaviors of S²PD treated alloys and provides potential applications in resource savings, alloy design, corrosion, biomimicry and other surface engineering areas.

2. Experimental

The material used in this work was a 7034-T6 aluminum alloy rod received from RSP Technology. Alloys were cut into 45 mm Ø specimens with thicknesses of 6 mm then grinded using 400# sand paper for the USSP treatment. The main alloying element composition provided by the manufacturer was Al-11Zn-2.3Mg-1.1Cu (in mass fraction). The schematic diagram of the S²PD (ultrasonic shot peening) setup has been illustrated elsewhere [21,23]. Specimens were fixed using a cylindrical enclosure made by cast iron with an inner diameter of 25 mm. The 4 mm Ø S440 stainless steel balls were used as shot peening media and powered by a titanium alloy horn connected with a VCF-1500 ultrasonic processor (Sonic & Materials, Newtown, CT) with a frequency of 20 kHz. The ultrasonic amplitude, the peak to peak, the up and down distance (excursion) that the horn tip travels was 56 μm. The peening distance was 10 mm and the peening duration was 8 min. During the S²PD treatment, the top surface of the horn was covered with a layer of shots.

XRD patterns of surfaces of the untreated and the S²PD treated AA 7034 were performed using a Bruker D-8 Focus X-ray diffractometer with CuK$_\alpha$ radiation and at a 2θ scanning rate of 4°/min to determine the phase constituent in the surface layer. The cross-section of the S²PD treated specimen was etched with Keller' reagent and then was characterized by Leica optical microscopy and Phenom Desktop scanning electron microscopy (SEM) with energy dispersive X-ray spectroscopy (EDS). The chemical composition change after the S²PD and one-year natural aging treatments was determined using EDS point and line scanning. Keysight G200 Nano Indenter was employed to measure micro-hardness and Young's modulus values of the surface layers of AA 7034 after the S²PD and one-year natural aging treatments. Indentation

tests were performed using Berkovich tips at a constant strain rate of 0.05 s⁻¹. The Poisson ratio of 0.3 and 5 s peak hold time were used. Hardness and Young's modulus are extracted from the load–displacement curves through Oliver-Pharr method.

The total broadening, β_{hkl}, which is the full width at half the maximum (FWHM) of a peak, can be described by Eq. (1) [24], from which the mean values of the microstrain and nanocrystalline grain size can be determined.

$$\beta_{hkl}^2 - \beta_0^2 = \left(\frac{K\lambda}{D_{hkl}\cos\theta} \right)^2 + (4\varepsilon\tan\theta)^2 \tag{1}$$

where β_0 is the instrumental broadening, K is a numerical factor frequently referred to as the crystallite-shape factor ($K = 0.89$ for Al), λ is the wavelength of incident wave, D_{hkl} is the crystallite size in the direction perpendicular to the lattice planes, hkl are the Miller indices of the planes being analyzed, θ is the Bragg angle, and ε is the microstrain. The curve of $\{\beta_{hkl}^2 - \beta_0^2\}$ as a function of θ can be plotted using all the diffraction peaks data. By fitting it using Eq. (1), the average grain size and the mean microstrain can be calculated.

The temperature dependence of the diffusion coefficient, D, is shown in Eq. (2):

$$D = D_0 \exp\left(\frac{Q_d}{RT} \right) \tag{2}$$

where

D_0, a temperature-independent preexponential (m²/s);
Q_d, the activation energy for diffusion (J/mol or eV/atom);
R, the gas constant, 8.31 J/mol K;
T, absolute temperature (K).

The needed diffusion time for elements can be roughly estimated using Zener's equation (Eqs. (3) and (4)) [25]:

$$S = \alpha_1 \sqrt{Dt} \tag{3}$$

$$\alpha_1 = (n_\infty - n_1)/\sqrt{(n_0 - n_1)(n_0 - n_\infty)} \tag{4}$$

where

S, the diffusion distance;
α_1, the growth coefficient;
n_∞, the concentration of the element in the matrix far away from the precipitate;
n_0, the concentration of the element in the precipitate;
n_1, the concentration of the element in the matrix that is in equilibrium with the precipitate.

3. Results and discussion

Fig. 1 shows the microstructure, XRD and nanoindentation results of the USSP treated AA 7034. The USSP affected depth was ∼200 μm as indicated by the cross sectional optical micrograph (Fig. 1a). The image reveals grain distortion caused by the USSP for the treated alloy. The original elongated grains of the as-received extruded bar were in the vertical direction (Area 1 in Fig. 1b). As the peened surface was approached (Areas 2 and 3 in Fig. 1b), the distribution of the elongated grains in the vertical direction gradually changed orientation to the horizontal direction along with a noticeable grain size reduction. Grain boundaries were absent in the SEM image for surface layers that had depths less than 40 μm (Area 4 in Fig. 1b). The lack of grain boundaries was due to the fact that the ultrafine/nano-sized grains on the topmost surface layer were too small to be detected by the SEM.

XRD was used to determine the mean grain size of nano-grains along with the microstrain of the peened surface layer (Fig. 1c). The
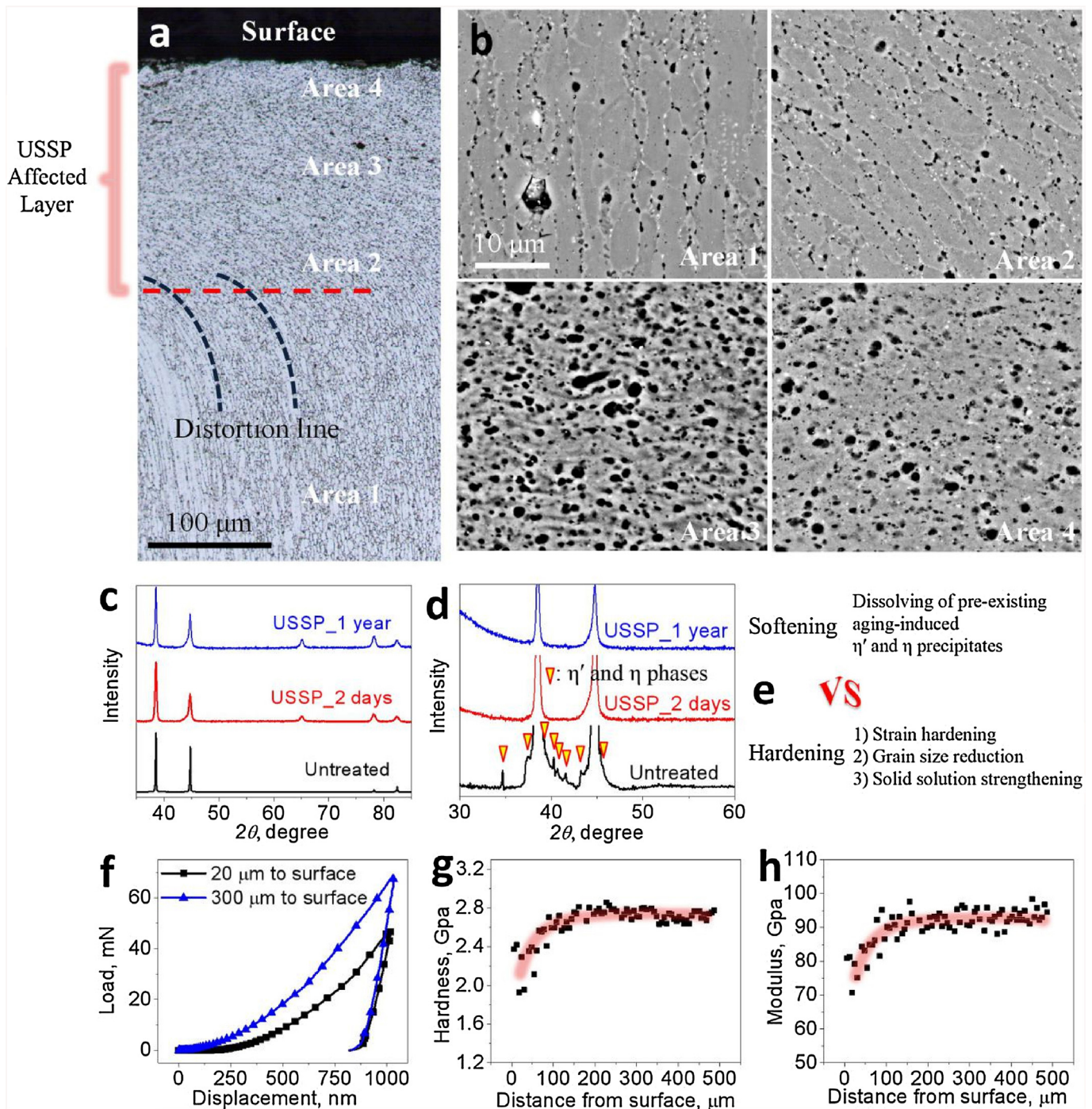
Fig. 1. Microstructure, XRD and nanoindentation results of USSP treated AA 7034. (a) Cross sectional optical micrograph of the USSP treated AA 7034. (b) SEM images of Areas 1~4 that were shown in Fig. 1a. The as-received alloy was an extruded bar with elongated grains in the vertical direction. Grain direction at Area 2 shifts approximately 45° compared to the original direction. For Area 3 with a depth of ~100 μm, elongated grains were in the horizontal direction along with grain size reduction. For the topmost surface layer with depths less than 40 μm (Area 4), grain boundaries were absent in the SEM. (c) XRD patterns of the as-received sample and the USSP treated samples. The average grain size and microstrain of the peened surface layers were derived from these patterns. (d) XRD patterns of the samples that show the dissolved pre-existing age-induced η′ and η precipitates after USSP. (e) Competing softening and hardening factors caused by USSP for AA 7034. (f) Load-displacement curves of nanoindentation for areas with different distances from the surface. Hardness (g) and Young's modulus (h) of peened AA 7034 as a function of distance from the surface that indicated both hardness and modulus decreased gradually as the alloy surface was approached.

peak broadening of the XRD image was a result of the microstrain and particle size reduction induced by the USSP. The affected thickness of the X-ray on the metal materials was seen to be as deep as 10 μm. Utilizing Eq. (1) (see Experimental section), the average grain size of the topmost layer of the two-day and one-year aged samples of the peened AA 7034 was determined as 23 nm and 28 nm, respectively. The mean microstrain of the topmost 10 μm

layer of the two-day and one-year aged samples of the peened AA 7034 was 0.20% and 0.16%, respectively. The comparison shows that the nanocrystalline structure on the surface layer was fairly stable during the yearlong natural aging treatment. In addition to the relative stability, the grain orientation of the sample was observed to be more random after USSP treatment. The nearly random orientation of peened samples was implied by its relative

intensities of diffraction peaks [21,26]. However, further pole figure characterization will be needed to expand on this observation.

Pre-existing ageing-induced η′ and η precipitates were found dissolved into the Al matrix after the USSP and two days of natural aging. The precipitates did not re-precipitate following the one-year exposure to an ambient environment (Fig. 1d). Thus, the current work was able to show homogenization of the microstructure of surface layer for the Al-Zn-Mg-Cu alloy. Nano-sized η′ and η precipitates, containing 31.5 at.% Zn, 28.6 at.% Mg 7.9 at.% Cu and balance of Al [27], were the major strengthening factors for the Al-Zn-Mg-Cu alloy due to the precipitates' extraordinary ability to hinder the movement of dislocations. Therefore, the post S²PD surface softening result was expected due to the dissolving of the η′ and η precipitates. However, S²PD is well-known for its surface hardening effect due to strain hardening, grain boundary hardening, and solid solution strengthening (Fig. 2b) [10,14,16]. The competitiveness of the softening and strengthening factors are shown in Fig. 1e. Surface hardness decreased from ~2.7 Gpa to ~2.2 Gpa, as confirmed by nanoindentation result (Fig. 1f and g). The Young's modulus of the peened layer also decreased after the treatment (Fig. 1h).

The decrease in surface hardness of the AA 7034 caused by the S²PD was the opposite of the usual results of many alloys treated in this way. The reason was believed to be the dissolving of pre-existing ageing-induced strengthening precipitates. The change in surface hardness depends on the hardening potential of the material as well as on the material condition before cold-working. For instance, in the case of a highly hardened initial condition, no additional increase in surface hardness can be achieved by mechanical surface treatment. Moreover, mechanical surface treatment of highly hardened metals might even result in a reduction of the surface hardness [28]. It should be noted that, the reduction in hardness of surface layer with a thickness of ~100 μm will usually not decrease the load-bearing capacity of the components especially for components with a relatively thick section.

The chemical composition of the mechanically deformed surface layer was compared to the substrate alloy composition. After USSP and one-year natural aging treatments, a gradient composition was observed. Element distribution as a function of distance from the surface of the untreated (Fig. 2a) and the USSP treated (Fig. 2b) AA 7034 were acquired using SEM-EDS line scan characterization. Both samples had the one-year natural aging before SEM-EDS line scan. The chemical composition did not change with the varying depths for the untreated sample but the peened sample showed segregated Zn and Cu along with depleted Mg on the alloy surface layer. EDS

point scan results (see Supplementary data Table S1) indicated that, for the topmost 1 μm surface layer, Zn content increased from 10.2 to 57.7 wt.% and Cu increased from 1.3 to 5.9 wt.%.

The XRD results indicated that the 57.7 wt.% Zn and 5.9 wt.% Cu on the topmost surface layer were in the form of solid solution (Fig. 1d). The values are significantly higher than the maximum solubility of Zn (2.3 wt.%) and Cu (0 wt.%) in the Al matrix under room temperature as predicted from the equilibrium phase diagrams [29]. On the opposite of Zn and Cu enrichments, Mg was depleted on the surface layer decreasing from 3.4 to 1.0 wt.%. The thickness of this particular chemical gradient within the peened specimen was 45 μm (45 μm for Zn and Mg, 30 μm for Cu), which is about ¼ of the USSP affected depth and comparable to the thickness of the gradient compositional layer usually found in biological materials [1,3–7].

The surface segregation and depletion are usually found in bulk metal surface. According to thermodynamics, the driving force of segregation is the decrease in surface Gibbs energy. For equilibrium segregation, the segregation depth should be in atom scale, which is from several Å to several nm. However, in the case of our study, the segregation depth about 45 μm indicates the compositional segregation is far away from the equilibrium state. The driving force of long distance segregation should be something else.

The solubility extension caused by high density of defects like vacancies, dislocations and grain boundaries can be explained using interfacial energy theory. Assuming a fine particle β dissolving into α matrix, and according to Gibbs-Thomson effect, the free energy increase due to interfacial energy is determined by Eq. (5) [30,31]:

$$\Delta G_\gamma = \frac{2\gamma V_m}{r} \qquad (5)$$

where γ is the α/β interfacial energy, V_m is the molar volume of the β phase, r is the radius of β phase. If β particle was surrounded by matrix with high density of defects like GBs, dislocations and vacancies, γ and thus ΔG_γ are expected to be increased. Thus, the solubility extension can be derived from molar free energy-composition diagram [31]. Therefore, through USSP by introducing a large number of defects like vacancies, dislocations and grain boundaries, solid solubility of Zn, Cu and Mg in Al matrix is expected to increase significantly, making the original supersaturated solid solution turns to be unsaturated. The dissolving of η′ and η precipitates confirms the transformation from supersaturation to unsaturation because the dissolution of second phase particles into unsaturated Al matrix is thermodynamically favorable. Driven by the decrease in Gibbs free energy of system, elements such as Zn,
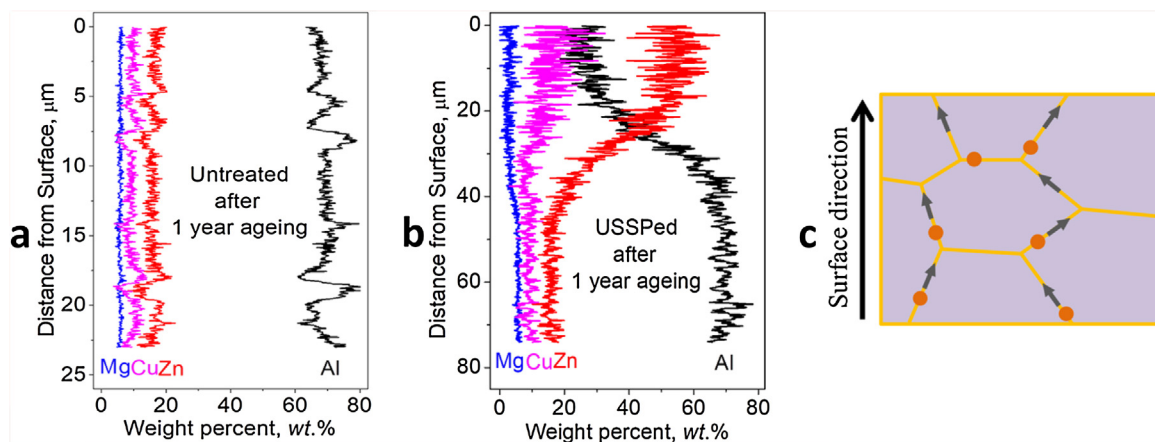

Fig. 2. Gradient chemical compositions of AA 7034 as a result of the USSP treatment and the following one-year natural aging. Element distribution as a function of distance from the surface for the untreated (a) and USSP treated (b) AA 7034 (both samples were treated with one-year natural aging). The resulting gradient compositional layer had a thickness of ~45 μm. (c) Schematic diagram of atoms diffusing along grain boundaries from sub-surface layer to surface layer.

Cu and Mg are expected to diffuse from sub-surface layer to surface layer.

The temperature dependence of the diffusion coefficient, D, is shown in Eq. (2) (see in Section 2). For Zn diffusing in the Al lattice, $D_0 = 3.0 \times 10^{-5}$ m^2/s, $Q_d = 121$ kJ/mol [32]. Extrapolation to 300 K gives the value of $D_{Zn} = 2.50 \times 10^{-26}$ m^2/s. Cu diffusion values in Al lattice are $D_0 = 6.5 \times 10^{-5}$ m^2/s, $Q_d = 136$ kJ/mol [32]. Extrapolation to 300 K gives the value of $D_{Cu} = 1.32 \times 10^{-28}$ m^2/s. If atom diffusion follows the lattice diffusion mechanism, the required diffusion time for elements can be roughly estimated using Zener's equation (Eqs. (3) and (4)) [25]. The result is that 8640 billion years would be needed for Zn to diffuse a distance of 45 μm and 316 trillion years for Cu diffuses a distance of 30 μm in Al lattice. The experimental diffusion duration is only one year. Apparently, an alternative diffusion mechanism must be responsible.

Diffusion along microstructural defects or so called "short circuit" paths, such as grain boundaries or dislocation pipes, is significantly faster than diffusion through an undisturbed crystal [33–35]. The ratio of diffusion enhancement can be up to several tens of orders of magnitude. The result of increased speed is that there are much higher concentrations of vacancies in microstructural defects than in the undisturbed crystal. By interchanging position with an adjacent vacancy, an atom moves. In most situations, short-circuit contributions to the overall diffusion flux are insignificant because the cross-sectional areas of these paths are extremely small. However, S^{2}PD creates very high density of grain boundaries, subgrain boundaries and/or twin grain boundaries and/or dislocation pipes on surface layer of alloys that leads to the short-circuit contributions becoming significant. The pipe-line feature caused by surface mechanical treatment has been utilized for fast diffusion of foreign atoms such as N [10], B [36], Ni [37], Cr [38], Zn [39], Al [40] and etc. from external sources into the alloys.

D_{Zn} along Al grain boundaries has been reported as 4.64×10^{-21} (subgrain boundary), 5.58×10^{-18} (high-angle GB with high activation energy), 5.08×10^{-15} (high-angle GB with low activation energy) [34] and 9.23×10^{-18} m^2/s [29]. D_{Cu} along Al grain boundary is 1.74×10^{-19} m^2/s as calculated from GB concentration profile in depth and 1.18×10^{-18} m^2/s calculated from the data of contour angle [41], and 5.77×10^{-19} m^2/s as estimated using Zener's equation [29]. For our case, according to Zener's equation, the estimated $D_{Zn} = 7.1 \times 10^{-15}$ m^2/s and $D_{Cu} = 1.4 \times 10^{-15}$ m^2/s. Both values are a little bit higher but at least comparable to the above literature data [29,34,41]. Therefore, as schematically shown in Fig. 2c, the diffusion along the "short circuit" paths such as grain boundaries is accountable for the long distance (45 μm) chemical gradient near alloy's surface. In contrast to the increase of Zn and Cu, Mg depletion was observed on the USSPed surface layer. The result might be due to the fact that Mg has a negative value of solute-vacancy binding energy [29], which leads to much slower diffusion kinetics than Zn and Cu.

The current work was able to observe that unique gradient microstructure and gradient chemical compositions can be obtained on an alloy treated with S^{2}PD and subsequent heat treatments. Fig. 3 shows a schematic diagram of the microstructure homogenization, grain refinement and gradient chemical composition of an Al-Zn-Mg-Cu alloy treated with S^{2}PD and natural ageing. Besides the current work's AA 7034, the phenomenon of gradient chemical compositions can be found in other 7000 series Al alloys, 2000 series Al alloys, stainless steel and brass (see Supplementary data Fig. S1). This indicates that long distance chemical gradient induced by S^{2}PD techniques is quite universal for treated alloys.

Another notable aspect of the current findings was that the layer with the gradient composition is as thick as 45 μm, which is comparable with that of biological materials such as mantis shrimp appendage [1,3,4] and spider fang [5]. During billions of years of evolution, biological materials have found the best way to
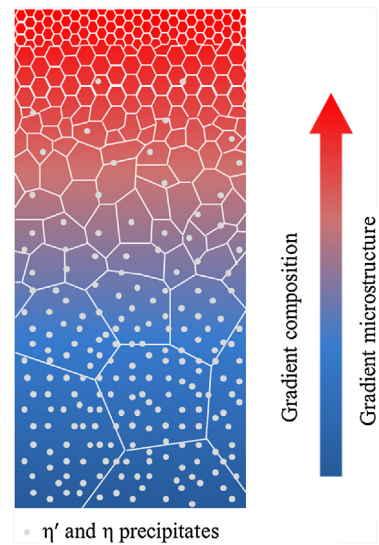

Fig. 3. Schematic diagram of a USSP & ageing treated Al-Zn-Mg-Cu alloy with gradient microstructure and gradient chemical composition in its near surface layer.

combine important physical properties through mixed gradients such as composition, dimension, arrangement, orientation and distribution. Although there is a long road ahead for material scientists to mimic biological materials, our finding provides a new possible way of fabricating structural materials with gradient chemical composition.

We also found surface softening effect for AA 7034 after S^{2}PD, mainly owing to the dissolving of pre-existing η' and η precipitates. However, rather than surface hardness and strength, the authors believe that the principal objective of the S^{2}PD technique is to fine tune the surface-related functional properties such as corrosion, fracture, fatigue, wettability, adsorption, catalytic activity and biocompatibility of alloys. All these surface-related properties are related with surface composition. A new design approach of metal alloys is inspired by this finding, which may find huge applications in corrosion protection of alloys and steels, resource saving and surface functionalization of materials, due to a long distance composition gradient can be created on the surface layer of alloys. Further investigation, calculation and simulations are needed to better understand diffusion mechanisms regarding this finding. Questions such as why segregation behavior differs in different alloy systems, how the diffusion driving force is influenced by the original composition and residual stress, and how elements in multi-component system interact with each other are out the scope of this communication, but will be addressed in the near future.

Contributions

Q. S. and Q. H. conceived this work and Q. H. directed the team. R. X. and K. Z. performed the Nano-indentation tests. Q. S. and R. X. analyzed the data and contributed equally. Q. S. wrote the manuscript, R. X., I. M. and Q. H. revised it.

Competing interests

The authors declare no competing financial interests.

Acknowledgements

analysis. The financial support of the China Scholarship Council is also gratefully acknowledged.

Appendix A. Supplementary data

Supplementary data associated with this article can be found, in the online version, at doi:10.1016/j.apmt.2018.12.002.

References

[1] Z. Liu, M.A. Meyers, Z. Zhang, R.O. Ritchie, Prog. Mater. Sci. 88 (2017) 467.
[2] U.G. Wegst, H. Bai, E. Saiz, A.P. Tomsia, R.O. Ritchie, Nat. Mater. 14 (2015) 23.
[3] S. Amini, A. Masic, L. Bertinetti, J.S. Teguh, J.S. Herrin, X. Zhu, H. Su, A. Miserez, Nat. Commun. 5 (2014) 4187.
[4] J.C. Weaver, G.W. Milliron, A. Miserez, K. Evans-Lutterodt, S. Herrera, I. Gallana, W.J. Mershon, B. Swanson, P. Zavattieri, E. DiMasi, Science 336 (2012) 1275.
[5] Y. Politi, M. Priewasser, E. Pippel, P. Zaslansky, J. Hartmann, S. Siegel, C. Li, F.G. Barth, P. Fratzl, Adv. Funct. Mater. 22 (2012) 2519.
[6] M.G. Pontin, D.N. Moses, J.H. Waite, F.W. Zok, PNAS 104 (2007) 13559.
[7] H. Peisker, J. Michels, S.N. Gorb, Nat. Commun. 4 (2013) 1661.
[8] D. Pender, N. Padture, A. Giannakopoulos, S. Suresh, Acta Mater. 49 (2001) 3255.
[9] A. Colli, A. Fasoli, C. Ronning, S. Pisana, S. Piscanec, A.C. Ferrari, Nano Lett. 8 (2008) 2188.
[10] W. Tong, N. Tao, Z. Wang, J. Lu, K. Lu, Science 299 (2003) 686.
[11] A.R. Studart, Chem. Soc. Rev. 45 (2016) 359.
[12] Z. Liu, Y. Zhu, D. Jiao, Z. Weng, Z. Zhang, R.O. Ritchie, Acta Biomater. 44 (2016) 31.
[13] X. Liu, H. Zhang, K. Lu, Science 342 (2013) 337.
[14] T. Fang, W. Li, N. Tao, K. Lu, Science 331 (2011) 1587.
[15] T. Roland, D. Retraint, K. Lu, J. Lu, Scr. Mater. 54 (2006) 1949.
[16] K. Lu, Science 345 (2014) 1455.
[17] V. Pandey, J. Singh, K. Chattopadhyay, N.S. Srinivas, V. Singh, J. Alloys Compd. 723 (2017) 826.
[18] X. Wu, N. Tao, Y. Hong, B. Xu, J. Lu, K. Lu, Acta Mater. 50 (2002) 2075.
[19] K. Lu, J. Lu, J. Mater. Sci. Technol. 15 (1999) 193.
[20] J.C. Villegas, L.L. Shaw, Acta Mater. 57 (2009) 5782.
[21] Q. Sun, Q. Han, X. Liu, W. Xu, J. Li, Surf. Coat. Technol. 328 (2017) 469.
[22] X. Li, K. Lu, Nat. Mater. 16 (2017) 700.
[23] Q. Sun, X. Liu, Q. Han, J. Li, R. Xu, K. Zhao, Surf. Coat. Technol. 337 (2018) 552.
[24] B.E. Warren, X-ray Diffraction, Dover Publication, INC., New York, 1990.
[25] C. Zener, J. Appl. Phys. 20 (1949) 950.
[26] Q. Sun, Q. Han, R. Xu, K. Zhao, J. Li, Corros. Sci. 130 (2018) 218.
[27] S. Wang, I. Huang, L. Yang, J. Jiang, J. Chen, S. Dai, D.N. Seidman, G. Frankel, L. Zhen, J. Electrochem. Soc. 162 (2015) C150.
[28] P. Hutmann, The application of mechanical surface treatment in the passenger car industry, in: L. Wagner (Ed.), Shot Peening, Wiley, Germany, 2006, pp. 1–12.
[29] S. Wang, J. Jiang, G. Fan, A. Panindre, G. Frankel, L. Zhen, Acta Mater. 131 (2017) 233.
[30] M. Perez, Scr. Mater. 52 (2005) 709.
[31] D.A. Porter, K.E. Easterling, M. Sherif, Phase Transformations in Metals and Alloys, CRC Press, New York, 2009.
[32] C. Smithells, Smithells Metals Reference Book, Butterworth-Heinemann, London, 1992.
[33] G. Stechauner, E. Kozeschnik, J. Mater. Eng. Perform. 23 (2014) 1576.
[34] D. Beke, I. Gödény, G. Erdelyi, F. Kedves, Philos. Mag. A 56 (1987) 659.
[35] T. Fujita, Z. Horita, T.G. Langdon, Philos. Mag. A 82 (2002) 2249.
[36] T. Balusamy, T.S. Narayanan, K. Ravichandran, Surf. Coat. Technol. 213 (2012) 221.
[37] Z. Wang, K. Lu, G. Wilde, S. Divinski, Appl. Phys. Lett. 93 (2008) 131904.
[38] Z. Wang, N. Tao, W. Tong, J. Lu, K. Lu, Acta Mater. 51 (2003) 4319.
[39] H. Wang, Z. Wang, K. Lu, Acta Mater. 60 (2012) 1762.
[40] S. Guo, Z. Wang, L. Wang, K. Lu, Surf. Coat. Technol. 258 (2014) 329.
[41] N. Dolgopolov, A. Rodin, A. Simanov, I. Gontar, Mater. Lett. 62 (2008) 4477.